Average and local atomic-scale structure in $BaZr_xTi_{1-x}O_3$ (x = 0. 10, 0.20, 0.40) ceramics by high-energy x-ray diffraction and Raman spectroscopy

2014 J. Phys.: Condens. Matter 26 065901

(http://iopscience.iop.org/0953-8984/26/6/065901)

IOP Publishing Journal of Physics: Condensed Matter
J. Phys.: Condens. Matter **26** (2014) 065901 (13pp) doi:10.1088/0953-8984/26/6/065901

Average and local atomic-scale structure in $BaZr_xTi_{1-x}O_3$ ($x = 0.10, 0.20, 0.40$) ceramics by high-energy x-ray diffraction and Raman spectroscopy

Vincenzo Buscaglia[1], Saurabh Tripathi[2], Valeri Petkov[2], Monica Dapiaggi[3], Marco Deluca[4,5], Andreja Gajović[6] and Yang Ren[7]

[1] Institute for Energetics and Interphases, National Research Council (IENI-CNR), Via De Marini 6, I-16149 Genova, Italy
[2] Department of Physics, Central Michigan University, Mount Pleasant, MI 48859, USA
[3] Dipartimento di Scienze della Terra, Università degli Studi di Milano, via Botticelli 23, I-20133 Milano, Italy
[4] Institut für Struktur- und Funktionskeramik, Montanuniversitaet Leoben, Peter Tunner Straße 5, A-8700 Leoben, Austria
[5] Materials Center Leoben Forschung GmbH, Roseggerstraße 12, A-8700 Leoben, Austria
[6] Molecular Physics Laboratory, Division of Materials Physics, Institute Rudjer Boskovic, Bijenicka 54, 10000 Zagreb, Croatia
[7] Advanced Photon Source, Argonne National Laboratory, Argonne, IL 60439, USA

E-mail: v.buscaglia@ge.ieni.cnr.it, saurabh14bhu@gmail.com and m.deluca@mcl.at

Received 18 October 2013, revised 3 December 2013
Accepted for publication 12 December 2013
Published 16 January 2014

Abstract

High-resolution x-ray diffraction (XRD), Raman spectroscopy and total scattering XRD coupled to atomic pair distribution function (PDF) analysis studies of the atomic-scale structure of archetypal $BaZr_xTi_{1-x}O_3$ ($x = 0.10, 0.20, 0.40$) ceramics are presented over a wide temperature range (100–450 K). For $x = 0.1$ and 0.2 the results reveal, well above the Curie temperature, the presence of Ti-rich polar clusters which are precursors of a long-range ferroelectric order observed below T_C. Polar nanoregions (PNRs) and relaxor behaviour are observed over the whole temperature range for $x = 0.4$. Irrespective of ceramic composition, the polar clusters are due to locally correlated off-centre displacement of Zr/Ti cations compatible with local rhombohedral symmetry. Formation of Zr-rich clusters is indicated by Raman spectroscopy for all compositions. Considering the isovalent substitution of Ti with Zr in $BaZr_xTi_{1-x}O_3$, the mechanism of formation and growth of the PNRs is not due to charge ordering and random fields, but rather to a reduction of the local strain promoted by the large difference in ion size between Zr^{4+} and Ti^{4+}. As a result, non-polar or weakly polar Zr-rich clusters and polar Ti-rich clusters are randomly distributed in a paraelectric lattice and the long-range ferroelectric order is disrupted with increasing Zr concentration.

Keywords: relaxors, $BaTiO_3$, Raman spectroscopy, high-energy XRD, polar nanoregions

(Some figures may appear in colour only in the online journal)

1. Introduction

The most widely used high-strain relaxor ferroelectrics nowadays are lead (Pb)-containing ABO_3 perovskites (see figure 1), such as $PbMg_{1/3}Nb_{2/3}O3$ (PMN) and $PbZn_{1/3}Nb_{2/3}O_3$ (PZN). They are characterized by (i) the existence of lattice disorder on the B-site, (ii) the presence of polar nanoregions (PNRs) at temperatures well above T_m, which

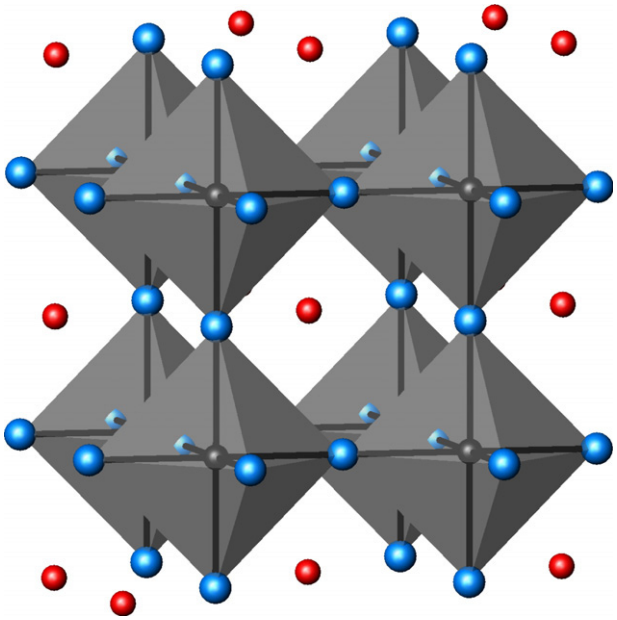

Figure 1. Fragment of the archetypal ABO_3 perovskite structure featuring a 3D network of corner shared B–O_6 octahedra and A ions (red circles) filling in the space between them. B ions are in black, oxygen ions are in blue.

is the temperature corresponding to the dielectric permittivity maximum, and (iii) the inclusion of these PNRs in a highly polarizable host lattice [1–3]. In these Pb-containing materials, compositional fluctuations on the B-site (e.g. Mg/Nb) induce charge disorder and random local electric fields which are thought to modify the long-range ferroelectric order. The size of the PNRs increases with decreasing temperature and, when $T \ll T_m$, one of two limiting phenomena are observed. If the polar domains become large enough and percolate the whole sample, a static, cooperative phase transition to a ferroelectric state occurs. On the other hand, if percolation of the polar domains does not take place, the slowing down of the PNRs dynamics results in a ferroelectric glass with randomly oriented polar domains. Currently there is a surge of interest in Pb-free (and thus environmentally friendly) materials showing properties comparable to Pb-based ceramics. Concerning Pb-free perovskite systems, $BaTiO_3$-based solid solutions such as (Ba, Sr)TiO_3, Ba(Ti, Zr)O_3 and Ba(Sn, Ti)O_3 are among the most widely investigated, due to the possibility to tailor ferroelectric properties by controlling the composition. $BaZr_xTi_{1-x}O_3$ (BZT), in particular, has attracted interest because of its very good dielectric properties, application in multilayer ceramic capacitors [1–9], and high tunability [10].

To understand better the very promising properties of BZT, detailed knowledge of the atomic-scale structure is needed. So far it is known that pure $BaTiO_3$ has a high-temperature paraelectric cubic-type structure of a perovskite-type (see figure 1), which at ∼125 °C changes into a tetragonal-type structure, rendering the material ferroelectric. At even lower temperatures $BaTiO_3$ exhibits phases with orthorhombic and rhombohedral symmetry. The lower symmetry phases are all ferroelectric and originate from small distortions of the prototype cubic structure related to off-centre displacement of Ti ions. In the mixed BZT ceramics with $x = 0.15$ and 0.20, a rhombohedral phase is suggested to exist at 80 K. On the other hand, only short-range polar order is proposed for $x = 0.35$ [11–13]. The appearance of a ferroelectric phase at low temperature when $x > 0.25$ is controversial. A pyroelectric current and hysteresis polarization loops with nonnegligible coercive fields have been found below 150–200 K [14, 15] for $BaZr_{0.35}Ti_{0.65}O_3$ ceramics. However, for the same composition, XRD experiments did not show the appearance of a long-range-ordered ferroelectric phase at 80 K [16] even after the application of an electric field, as observed in other relaxors. A further peculiarity of $BaZr_{0.35}Ti_{0.65}O_3$ is the absence of a heat capacity anomaly expected from the freezing of the PNRs [17]. On the basis of a detailed dielectric spectroscopy investigation it has been proposed that at low temperature a 'quasi-ferroelectric' state exists when $x = 0.325$ [18]. Recent nonlinear permittivity measurements [19] indicate a ferroelectric phase transition for $x = 0.25$, a relaxor state for $x = 0.35$ and a mixed behaviour for $x = 0.30$.

From the foregoing discussion, it is evident that the understanding of the ferroelectric properties and the respective atomic-scale structure of $BaZr_xTi_{1-x}O_3$ ceramics with x varying from 0.10 to 0.40 as a function of composition and temperature is still incomplete.

Conventional XRD and Rietveld analyses can provide useful insight into the long-range BZT crystal structure as it changes with the Zr/Ti ratio. On the other hand, techniques such as total XRD scattering coupled to atomic pair distribution function (PDF) analysis [20, 21] and Raman spectroscopy [11–13, 22–32] can provide knowledge about the short-to-medium-range order structural features of BZT and other ferroelectric oxides. Here we apply a combination of conventional XRD, atomic PDFs analysis and Raman experiments to reveal more clearly the atomic ordering of $BaZr_xTi_{1-x}O_3$ ceramics with $x = 0.10$ (considered to correspond to a conventional ferroelectric state), 0.2 (considered to correspond to an intermediate diffuse transition state) and 0.4 (considered to correspond to a relaxor-type state), including the temperature and composition driven evolution of the underlying perovskite-type structure and the local disorder in it.

2. Experimental details

2.1. Synthesis

$BaZr_xTi_{1-x}O_3$ ceramics ($x = 0.10$, 0.20 and 0.40) were prepared by a solid-state route using nanocrystalline raw materials to achieve lower reaction temperatures and high chemical homogeneity of the final BZT materials. The precursor powders were characterized by measuring their specific surface area using the nitrogen adsorption method. In a typical synthesis, stoichiometric amounts of TiO_2 (Grade Aeroxide P25, Evonik Degussa GmbH, Hanau, Germany, $S_{BET} = 55\ m^2\ g^{-1}$, $d_{BET} = 28$ nm), ZrO_2 (Grade TZ0, Tosoh, Japan, $S_{BET} = 15.3\ m^2\ g^{-1}$, $d_{BET} = 67$ nm) and $BaCO_3$ (Solvay Bario e Derivati, Massa, Italy, $S_{BET} = 27.6\ m^2\ g^{-1}$, $d_{BET} = 55$ nm) were wet mixed in water using zirconia media. A solution of ammonium polyacrylate was prepared by titrating an aqueous solution of

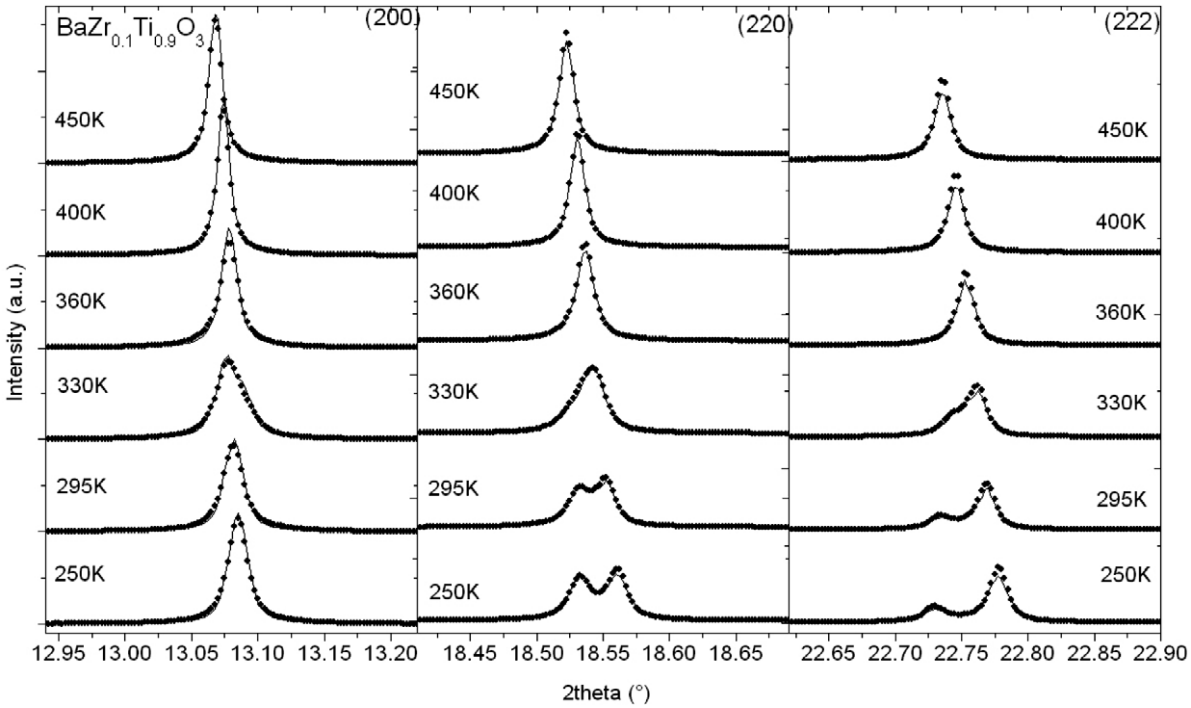

Figure 2. Experimental (dots) and Rietveld fit (line) XRD patterns of $BaZr_xTi_{1-x}O_3$ ceramics with $x = 0.10$. The fits and the disappearing of the splitting of (220) and (222) Bragg peaks with increasing temperature clearly show that the low-temperature rhombohedral structure of BZT transforms into a cubic structure, passing through an orthorhombic structure at 330 K.

polyacrylic acid (Acros Chimica, Milan, Italy, MW2000) up to pH 10 and added as a dispersant. The dried mixed powders were calcined for 4 h at 1273 K, wet milled to disintegrate the agglomerates and finally freeze-dried and sieved. Cylindrical green bodies of BZT (diameter ∼1 cm, length ∼1 cm) were prepared by cold isostatic pressing and sintered for 4 h at 1773 K in air. Sample density was measured by immersion in water using the Archimedes method. The thus-obtained bulk ceramics were quite dense (97–98% rel. density), with only a limited intergranular porosity and a grain size of 3–5 μm for $x = 0.10$ and 0.20 and 1–2 μm for $x = 0.40$. Secondary phases were not detected by backscattered imaging in a scanning electron microscope (SEM-BS) and conventional XRD.

2.2. High-resolution powder XRD and Rietveld analysis

High-resolution powder XRD data for $BaZr_xTi_{1-x}O_3$ ($x =$ 0.10, 0.20, 0.40) were obtained at the beam-line 11-BM at the Advanced Photon Source, Argonne National Laboratory. Fine powder samples obtained by grinding the bulk ceramic samples were sealed in Kapton capillaries and measured in steps of 0.0025° (2θ) using x-rays with a wavelength of 0.4587 Å. A multi-analyser detection assembly, consisting of 12 independent Si(111) crystals and $LaCl_3$ scintillation detectors, was used to detect the scattered x-ray intensities. XRD data were taken at several temperatures (100–450 K) using an Oxford Cryostream 700+ gas blower up to wavevectors of approximately 12 $Å^{-1}$. The diffraction patterns showed very sharp and narrow peaks, indicative of good crystallinity and chemical homogeneity.

The experimental XRD data sets were subjected to Rietveld refinements (see figures 2–4). The refinements were performed using the EXPGUI program suite [33, 34]. The refinements started from the highest temperature data sets having a cubic crystallographic symmetry. The change in symmetry could not be always easily detected, as the distortions from the high-temperature cubic structure often turned out to be very small. Accordingly, the symmetry of the model was changed whenever the Rietveld goodness of fit parameter (R_{wp}) became substantially larger than that of the model with a lower crystallographic symmetry. The number of refined structure-related parameters could not be kept exactly the same between the different refinements due to the change in the crystallographic symmetry. However, XRD peak profile and background parameters were kept the same with all refinements. The crystallographic symmetry of the models explored was: cubic (SG $Pm3m$), orthorhombic (SG $Amm2$), and rhombohedral (SG $R3m$). In some cases a tetragonal model (SG $P4mmm$) was tried, but it did not converge in the refinements. In total, the respective lattice parameters, XRD peak profile and background parameters, the Ba, Ti/Zr and O thermal parameters as well as the Zr occupancy were refined. The latter was refined as a check of the samples' composition and always found to be within ±0.05 of the nominal composition. The refined thermal parameters increased monotonically with temperature, as expected, and had reasonable values for all Rietveld refined XRD data sets.

2.3. High-energy XRD and atomic pair distribution analysis

High-energy XRD data were obtained at the beam-line 11-ID-C at the Advanced Photon Source, Argonne National

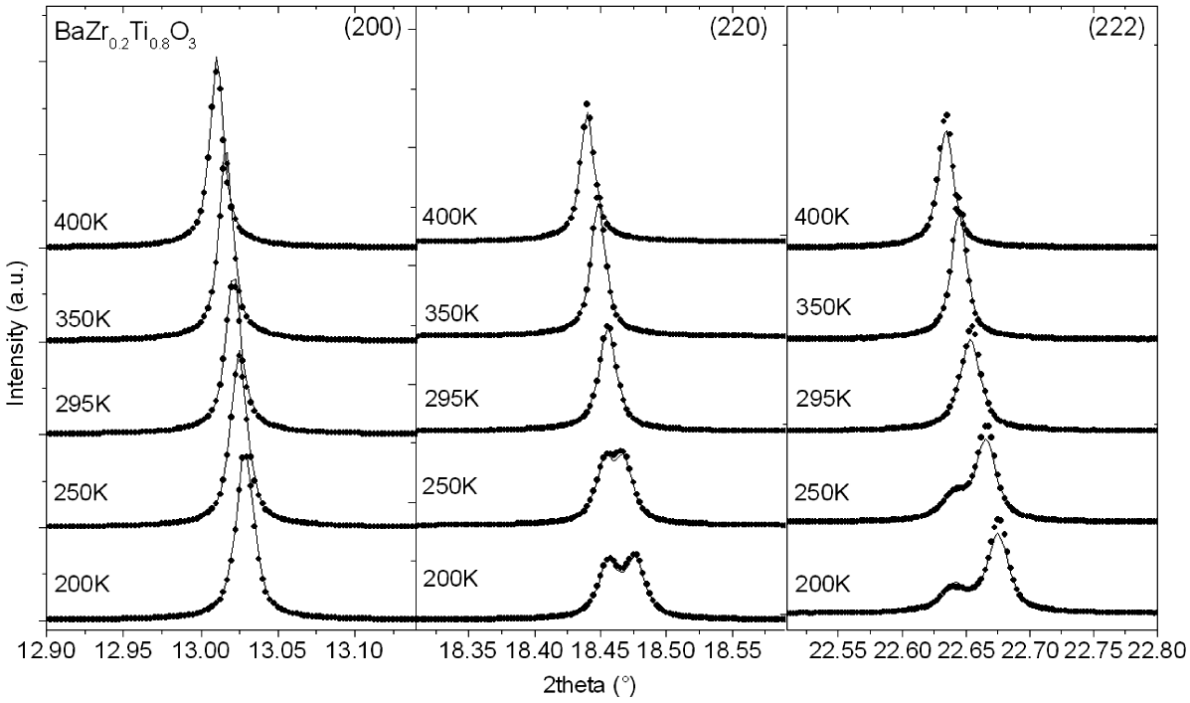

Figure 3. Experimental (dots) and Rietveld fit (line) XRD patterns of $BaZr_xTi_{1-x}O_3$ ceramics with $x = 0.20$. The fits and the disappearing of the splitting of (220) and (222) Bragg peaks clearly show that the low-temperature rhombohedral structure of BZT transforms into a cubic structure with increasing temperature.

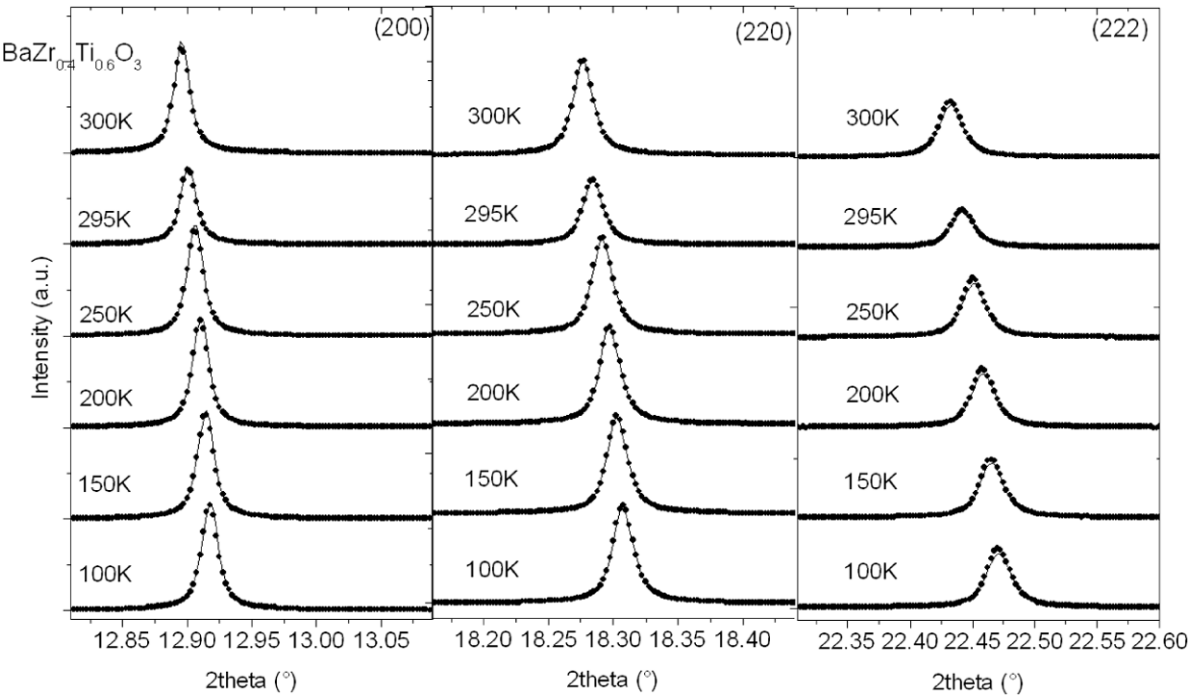

Figure 4. Experimental (dots) and Rietveld fit (line) XRD patterns of $BaZr_xTi_{1-x}O_3$ ceramics with $x = 0.40$. The fits show that the BZT structure type remains (pseudo) cubic, since no splitting of (220) and (222) Bragg peaks can be seen at any temperature.

Laboratory. The same samples used for high-resolution XRD studies were measured using x-rays of wavelength 0.1080 Å and an area detector (PerkinElmer). Data were taken at several temperatures (100–450 K) using an Oxford Cryostream 700+ gas blower. The datasets were collected to wavevectors of approximately 30 $Å^{-1}$ and then converted to absolute (electron) units into the so-called structure functions, $S(q)$ [35, 36] related to only the coherent part of the diffraction

pattern, $I^{\mathrm{coh}}(Q)$, as follows:

$$S(Q) = 1 + \left[I^{\mathrm{coh}}(Q) - \sum c_i |f_i(Q)|^2\right] \Big/ \left|\sum c_i f_i(Q)\right|^2, \quad (1)$$

where c_i and $f_i(Q)$ are the atomic concentration and x-ray scattering factor respectively for the atomic species of type i. Here Q is the wavevector ($Q = 4\pi \sin\theta/\lambda$), where 2θ is the angle between the incoming and outgoing x-rays and λ is the wavelength of the x-rays used. The structure factors were Fourier transformed to the so-called atomic pair distribution functions (PDFs), $G(r)$, as follows:

$$G(r) = \frac{2}{\pi} \int_{Q=o}^{Q_{\max}} Q[S(Q) - 1] \sin(Qr)\, \mathrm{d}Q. \quad (2)$$

The reduction of the diffraction data to structure factors and then to atomic PDFs was done with the help of the program RAD [37]. The advantage of considering the high-energy XRD data in real space is that atomic PDFs (i) take into account both Bragg peaks and diffuse scattering components in the XRD patterns and (ii) so reflect both the short- and long-range atomic ordering in BZT ceramics. This, coupled with the high value of the wavevectors reached, allows fine features of the atomic-scale structure to be revealed, including the presence of local atomic disorder, as several studies have already shown [38–40].

2.4. Raman spectroscopy

Raman spectra were obtained with a research-grade micro-Raman spectrometer (T64000, Horiba/Jobin-Yvon, Villeneuve d'Ascq, France) using a 514.5 nm Ar-ion laser (Coherent Innova 400, Coherent, Santa Clara, CA, USA) as an excitation source. The laser light was focused on the sample surface by means of a long working distance 50× objective lens with a numerical aperture (NA) = 0.5 (Olympus, Tokyo, Japan). The nominal power of the laser was set to 20 mW. Spectra were collected in a true backscattering geometry with the aid of a liquid nitrogen-cooled charged coupled device (CCD) camera. Temperature-dependent (*in situ*) Raman experiments were performed by means of a Linkam THMS600 heating–cooling stage (Linkam, Tadworth, UK). Also, spectra were collected in a triple subtractive configuration, in order to allow measurements in the low-wavenumber region (∼50 cm^{-1}) by spatial filtering. The collected spectra were analysed by commercial software (Labspec 4.02, Jobin-Yvon/Horiba) using multiple Gaussian–Lorentzian peak functions.

3. Results and discussion

3.1. High-resolution XRD data and Rietveld refinement

$BaTiO_3$, $BaZrO_3$ and mixed BZT adopt a perovskite-type structure (see figure 1). $BaZrO_3$ is a weak incipient ferroelectric whose dielectric permittivity increases gradually with decreasing temperature, and is cubic at all temperatures [15]. Pure $BaTiO_3$ shows three distinct phase transitions, rhombohedral (R)–orthorhombic (O) at about 183 K, orthorhombic (O)–tetragonal (T) at about 278 K, and tetragonal (T)–cubic (C) at ∼398 K, due to hardening of a soft polar phonon corresponding to the centre of the cubic Brillouin zone with ($k = 000$). These phase transitions are characterized with a displacement of Ti ions along the [001], [110] and [111] directions of the pseudocubic perovskite unit cell, resulting in the appearance of a net polarization axis, leading to ferroelectric tetragonal, orthorhombic and rhombohedral phases, respectively. The T–C transition temperature (398 K) corresponds to the Curie point, T_C, above which $BaTiO_3$ is in a paraelectric state. It is important to note that Ti ions exhibit local off-centre ⟨111⟩-type displacements even above T_C [41, 42], rendering the local atomic ordering in $BaTiO_3$ different from the average cubic-type structure as evidenced by diffuse scattering [41–43], nuclear magnetic resonance [44, 45] and x-ray absorption [42] studies.

Dielectric measurements have indicated that the phase transition sequence of $BaTiO_3$ is more or less preserved in $BaZr_xTi_{(1-x)}O_3$ when $x < 0.15$. These measurements also indicate that the T–C phase transition temperature decreases with increasing Zr content whereas the temperatures corresponding to the R–O and O–T phase transitions increase with increasing x. Accordingly, when $x = 0.10$, our XRD data taken at 400, 450 and 360 K are well approximated by the cubic model, at 330 K by the orthorhombic model and at 250 and 295 K by a rhombohedral-type model (see figure 2 and table 1). The fit for $T \leq 360$ K is of slightly inferior quality, but the reason for this behaviour is unclear. Prior studies have found that in BZT with $x = 0.10$–0.15, the three (C–T, T–O, O–R) transitions observed in $BaTiO_3$ merge together, as evidenced by a single broad permittivity peak with a maximum at ∼343 K [4, 15]. A second-order-like, diffuse ferroelectric transition from the R to the C phase is reported for $0.15 < x < 0.25$. In agreement with these studies, the structure of our sample with $x = 0.20$ was found to be rhombohedral at 200 and 250 K, and cubic at 295, 350 and 400 K (see figure 3). A certain ambiguity was experienced with the XRD data at 295 K: two of the Rietveld refinements provided R_{wp} very close to each other (table 1). Preference was given to a cubic model with $R_{\mathrm{wp}} = 8.25\%$. The ambiguity indicated a possible phase coexistence of lower (R) and higher symmetry (C) BZT phases, a rather common situation in ferroelectric solid solutions near phase transitions.

For $0.25 < x < 0.75$, $BaZr_xTi_{1-x}O_3$ system has been found to exhibit a relaxor-type behaviour, evidenced by a strong frequency dependence of the dielectric permittivity peak [15, 18, 46]. The refinement of our XRD data for $x = 0.40$ indicated an average (pseudo)cubic structure typical of relaxor ferroelectrics at all temperatures assessed in our study: neither splitting nor evident Bragg peak asymmetries were observed in the respective XRD patterns (see figure 4).

The temperature dependence of the unit cell volume for $BaZr_xTi_{1-x}O_3$ ceramics as determined by the results of Rietveld refinements carried out by us is reported in figure 5. The volume clearly shows an anomaly at the ferroelectric–paraelectric transition temperatures for $x = 0.10$. The anomaly is much less evident for $x = 0.20$ and this correlates with the existence of a diffuse phase transition. A nonlinear temperature dependence without anomalies is observed for the $x = 0.40$ sample. The latter may be considered a signature of a relaxor-type behaviour involving an increase of the volume fraction of

Table 1. R_{wp} values for the various Rietveld fits of the XRD patterns of the different BZT samples. The last column shows the cell parameters corresponding to the structure with lowest R_{wp}.

Temperature (K)	R_{wp} (%) (cubic)	R_{wp} (%) (orthorhombic)	R_{wp} (%) (rhombohedral)	Cell parameters
		$x = 0.10$		
250			11.81	$a = 4.025\,700(6)$
				$\alpha = 89.914$
295			11.57	$a = 4.026\,710(4)$
				$\alpha = 89.938$
330	18.33	10.91	15.88	$a = 4.024\,29(1)$
				$b = 5.699\,94(2)$
				$c = 5.695\,06(2)$
360	11.32	12.66		$a = 4.028\,000(2)$
400	8.76			$a = 4.029\,280(2)$
450	8.41			$a = 4.031\,020(3)$
		$x = 0.20$		
200			8.98	$a = 4.043\,170(2)$
				$\alpha = 89.937$
250			8.49	$a = 4.044\,370(3)$
				$\alpha = 89.955$
295	8.25	9.20	8.76	$a = 4.045\,460(4)$
350	8.87			$a = 4.047\,140(2)$
400	8.22			$a = 4.048\,950(3)$
		$x = 0.40$		
100	8.48			$a = 4.077\,950(4)$
150	8.42			$a = 4.078\,952(4)$
200	8.25			$a = 4.080\,320(2)$
250	7.38			$a = 4.081\,620(2)$
295	7.71			$a = 4.083\,220(2)$
350	7.20			$a = 4.084\,900(2)$

polar nanoregions with decreasing temperature. The sequence of phase transitions was more clearly revealed by Raman scattering.

3.2. Raman scattering

In the cubic (C) paraelectric phase of pure $BaTiO_3$ (BT)—above T_C—using the traditional group theory analysis normal optical modes would consist of three IR-active F_{1u} modes and a silent F_{2u} mode [47], all Raman-inactive. Well above T_C, however, several studies reported the presence of broad Raman lines (at around 225 and 520 cm^{-1}) in the spectrum of BT [23, 48–50]. Those have been interpreted as being activated by local short-range distortions due to off-site displacements of Ti ions across neighbouring crystallographic sites [51]. In fact, in BT the paraelectric-to-ferroelectric transition is a combination of displacive and order–disorder type, as evidenced by both experimental [52, 53] and theoretical [54] studies.

Upon transition to the ferroelectric tetragonal phase, according to group theory, each F_{1u} mode transforms into A_1 and E modes, whereas the F_{2u} mode gives rise to B_1 (silent) and E modes, which can be clearly assigned only by polarization measurements in single crystals [47, 55]. In randomly oriented polycrystalline ceramics the directions of phonon wavevectors are randomly distributed with respect to the crystallographic axes, and thus quasimodes rather than polar phonons are observed. Raman lines appear broad and none of them possesses true A_1, E or B_1 symmetry [56, 57]. This picture is further complicated in B-site-substituted BZT ceramics, since a relaxation of the selection rules is expected in the presence of compositional disorder. The solid solutions studied by us involve Zr^{4+} and Ti^{4+} cations, which have different ionic radii of 0.72 and 0.605 Å, respectively. The difference leads to a coexistence of two local octahedral environments in the perovskite structure of BZT. According to recent EXAFS and neutron diffraction experiments the TiO_6 and ZrO_6 octahedra in BZT preserve their individuality and so the Ti–O and Zr–O distances appear similar to those observed in pure $BaTiO_3$ and $BaZrO_3$ [58, 59]. The resulting local structural distortions produce (i) the appearance of extra-Raman modes, interference effects and further spectral broadening, and (ii) a shift in the positions of the Raman peaks. All these complicate further the interpretation of the Raman spectra of BZT ceramics. Accordingly, the Raman spectra presented here are discussed in terms of spectral features without referencing to particular polar phonons. Note, qualitative reasoning based on ion masses, sizes, and two-mode behaviour, i.e. hard-mode spectroscopy [60–62] is still possible in this case.

Raman spectra of $BaZr_xTi_{1-x}O_3$ ceramics with $x = 0.10$, 0.20, and 0.40 at 118 K are shown in figure 6. Observed spectral features are numbered consecutively from 1 to 11, starting from the low-wavenumber region. The spectrum of $BaZr_{0.10}Ti_{0.90}O_3$ resembles that of a rhombohedral BT material [12], except for the larger broadening associated with the presence of compositional disorder. Peaks 6, 7, 9 and 10 are

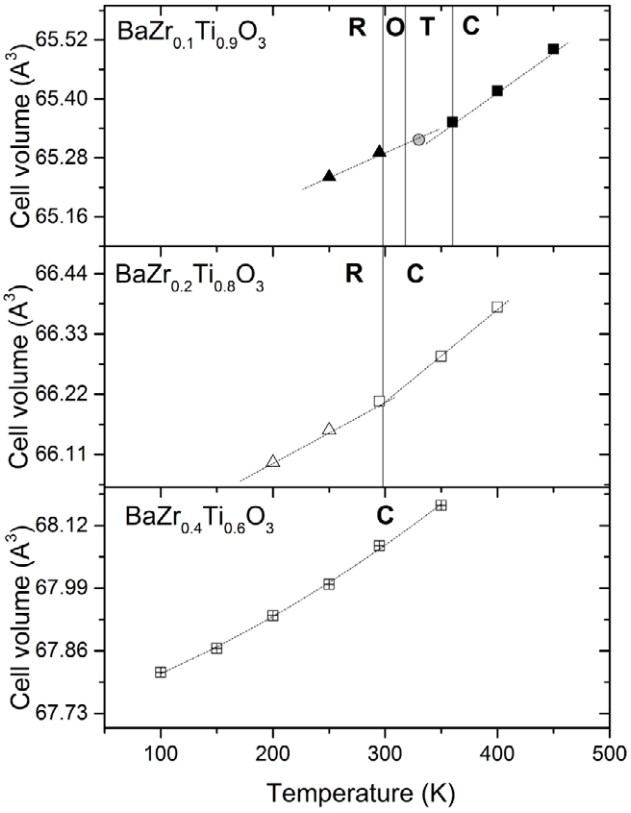

Figure 5. Volume of the unit cell for $BaZr_xTi_{1-x}O_3$ ceramics with $x = 0.10$ (top), $x = 0.2$ (middle) and $x = 0.4$ (bottom) as a function of temperature. Squares (crossed, empty, filled): cubic structure. Triangles (empty, filled): rhombohedral structure. Circles: orthorhombic structure. Dashed lines are a guide to the eye. Vertical solid lines mark the position of the phase transition as determined by Raman scattering (phases described by capital letters). In the $x = 0.40$ sample no clear phase transition is observed.

found in all ferroelectric phases of BT-based materials. Peaks 6 and 9 have a dominant A_1(TO) character, as was proven in polycrystalline BT by polarization measurements [63, 64], and the former is associated with polar Ti–O vibrations. Peak 10 is due to a bending and stretching of BO_6 octahedra and so has a mixed A_1 and E character [29, 65], whereas peak 7 is the 'silent' mode [47]. Another feature that appears in all ferroelectric phases of BT is the interference dip (4) at ∼180 cm^{-1}. This was reported as being caused by antiresonance between the narrow $A_1(TO_1)$ and broad $A_1(TO_2)$ modes [66]. An alternative explanation invokes an anharmonic coupling of three A_1 phonons [67, 68]. The presence of rhombohedral symmetry is indicated by the coexistence of peaks 1, 3, 5 (the so-called 'triple mode' [12, 32]), by the small peak 8 at ∼490 cm^{-1} [69], and by the absence of the overdamped soft mode [30]. The presence of peak 1 at ∼119 cm^{-1} is related to Zr–O motion in BZT and regarded as an indicator of the presence of nanometre-sized Zr-based clusters with local rhombohedral-type structure [13, 29]. This two-mode behaviour is possible only if local Zr-based domains extend over tens of unit cells, so that the phonon lifetime (scattering coherence) can give rise to a definite Raman peak [13, 62]. Features 2 and 11 are present only in BZT solid solutions. The former is an interference effect between A_1(TO) phonons

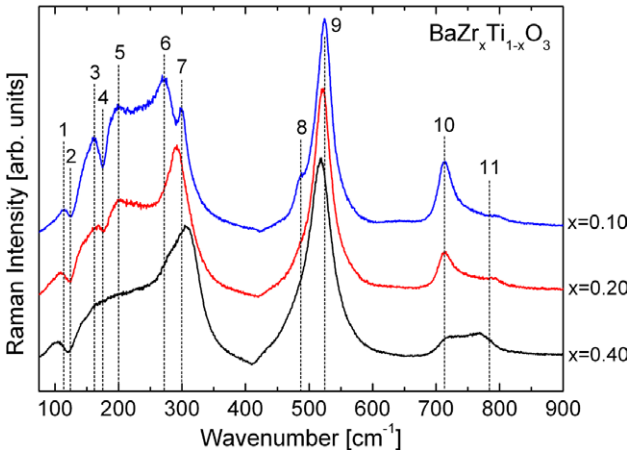

Figure 6. Raman spectra of $BaZr_xTi_{1-x}O_3$ ($x = 0.10$, 0.20 and 0.40) collected at 118 K. The spectra show the characteristic features of B-site-substituted $BaTiO_3$ solid solutions. Raman features are numbered consecutively from 1 to 11, starting from low wavenumbers (see text).

and appears when two chemically different BO_6 octahedral environments coexist in the perovskite structure [31, 70]. Its strength may be related to the amount of substituted B-type cations. Similarly to feature 1 it indicates the presence of nanosized ordered Zr-rich clusters in the perovskite structure [62]. Feature 11 results from the presence of B- or A-sites occupied by cations of different sizes [13, 32, 65]. This mode has been previously considered as an indicator of relaxor behaviour [29]. Although A- and B-site-substituted BT does display relaxor behaviour for sufficient substituent content, this mode appears also for dopant concentrations lower than the crossover to the relaxor state [32, 71].

Upon increasing Zr content from $x = 0.10$ to 0.20 and then to $x = 0.40$ (cf figure 6) several changes in the Raman spectra taken at 118 K appear. First, the 'triple mode' below 250 cm^{-1} progressively disappears, together with the interference dip at 180 cm^{-1} and the mode 8 at ∼490 cm^{-1}. This suggests that the rhombohedral symmetry is gradually lost, indicating a mixed R–C structure. The 'silent' mode at ∼305 cm^{-1} disappears for $x \geq 0.2$. This, however, is not necessarily an indication of a loss of the BZT ferroelectric character. As a matter of fact its disappearance could result from the shift of the mode 6 at ∼270 cm^{-1} towards higher wavenumbers. Such an effect has been already observed in Zr- [32] and Bi-substituted BT [72, 73] and related to the change in the interatomic forces due to chemical substitution. Therefore, it is not possible to say clearly if $BaZr_{0.20}Ti_{0.80}O_3$ is or is not in a ferroelectric state judging on the 'silent' mode alone; the fact that both the interference effects at ∼180 cm^{-1} and the mode 10 at ∼715 cm^{-1} are observed indeed hints to the presence of a long-range ferroelectric state. Mode 10 can be used as a ferroelectricity index, as explained later. Concerning the $x = 0.40$ composition, the interference Raman feature (mode 4) is not present and Raman mode 10 appears with a much lower intensity. This, together with the absence of the 'silent' Raman mode, suggests that the material has predominantly cubic-type structure, in line with the results

from Rietveld refinements. The observed Raman spectrum is indeed consistent with the presence of a highly disordered cubic structure, which is also hinted at by the very prominent dip (2) at ∼125 cm^{-1}. The presence of this feature may be due to ordered Zr-rich regions that are coherent on a scale larger than that exhibited by the other samples.

Temperature-dependent Raman spectra of all the $BaZr_xTi_{1-x}O_3$ ceramics studied here are presented in figure 7. All compositions show a Raman spectrum well above T_C, i.e. in the cubic paraelectric phase, confirming the presence of local regions with short-range atomic disorder. The same Raman features are also observed in the paraelectric phase of BT. The Raman spectra of BZT with $x = 0.10$ shows R symmetry up to room temperature. Above this temperature the Raman spectrum resembles that of the O phase of BT (absence of the 'triple mode', shift of the peak at ∼490 cm^{-1}, persistence of feature 5). When the temperature is raised further to above 318 K the spectrum starts resembling that of the T phase of BT (shift of the mode at 270 cm^{-1} to higher wavenumbers). A coexistence of O-type and T-type phases cannot be excluded in this temperature range. The transition to the cubic phase is diffuse, which may be expected for a solid solution and is completed by 358 K, as signalled by the simultaneous disappearance of the interference dip at ∼180 cm^{-1}, the 'silent' mode at ∼305 cm^{-1} and the mode at ∼715 cm^{-1}. This phase sequence is in accord with other studies on $BaZr_xTi_{1-x}O_3$ [29, 32, 15], and with the results of Rietveld refinements (figure 5). Upon increasing the Zr content ($x = 0.20$) Raman data suggest a coexistence of R-type and C-type phases at room temperature. Here the transition to the paraelectric (C-type) phase appears quite diffuse. The absence of the 'silent' mode complicates the observation of the ferroelectric-to-paraelectric transition for BZT with $x = 0.2$. However, the simultaneous disappearance of the dip at ∼180 cm^{-1} and the mode at ∼715 cm^{-1} at around room temperature suggests that the transition takes place above 300 K, in agreement with the XRD data. A very different picture emerges when the evolution of the Raman spectrum of $BaZr_{0.40}Ti_{0.60}O_3$ with temperature is examined (cf figure 7(c)). Raman peaks belonging to R-type symmetry are not seen for the whole temperature range covered in our study, including the 'ferroelectric' Raman features (4), (7) and (10). In addition, the Raman spectra for the different temperatures look alike, that is, no ferroelectric-to-paraelectric transition is detected by Raman spectroscopy. This, together with the prominent dip at 125 cm^{-1} (which indicates B-site cation ordering), hints to a possible relaxor state and corresponding (pseudo-)cubic structure for BZT with $x = 0.4$. Cation ordering and the absence of a clear structural phase transition are in fact characteristics of relaxor systems, in which the dielectric dynamics can be explained in terms of growing and shrinking of polar nanoregions (PNRs) [31, 74]. Note, our Rietveld refinements also hint at the presence of a relaxor state in BZT with $x = 0.40$ (see the temperature behaviour of the unit cell volume in figure 5).

The transition from the ferroelectric to the paraelectric state and the crossover to the relaxor behaviour can be detected by monitoring the relative intensity of Raman features

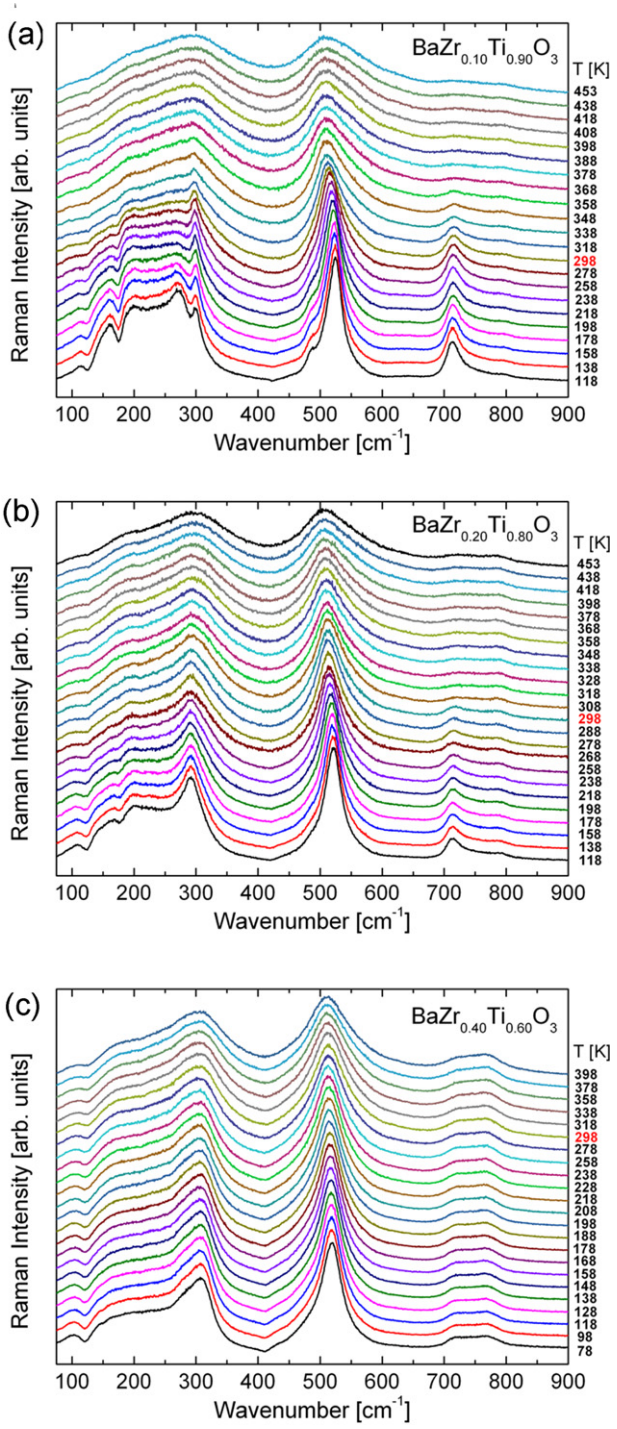

Figure 7. Temperature-dependent Raman spectra of $BaZr_xTi_{1-x}O_3$ compositions: (a) $x = 0.10$, (b) $x = 0.20$ and (c) $x = 0.40$. Ferroelectric order is clearly recognizable in $BaZr_{0.10}Ti_{0.90}O_3$. For the $x = 0.20$ composition ferroelectric order occurs below 298 K, whereas for $x = 0.40$ no transition appears and the overall spectral signature suggests a relaxor-type state.

(10) and (11) (cf figure 7). The mode (10) at ∼715 cm^{-1} is in fact a mixed A_1 and E mode associated with the breathing of BO_6 octahedra in the ferroelectric phase [65, 69], whereas the mode (11) at ∼780 cm^{-1} is a stretching mode of BO_6 octahedra related to A- or B-site substitutions in the perovskite structure. The latter may appear regardless

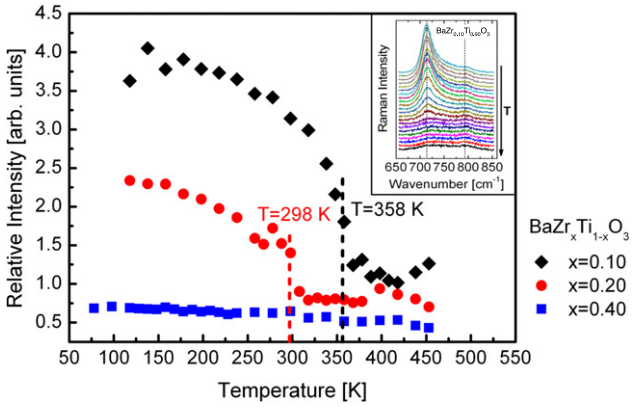

Figure 8. I_{715}/I_{780} intensity ratio in dependence of temperature for all investigated BZT compositions. Samples with $x = 0.10$ and 0.20 show an abrupt relative intensity drop indicative of a ferroelectric-to-paraelectric transition. For $x = 0.40$, no transition is detected. The inset shows the high-frequency portion of the Raman spectrum of $BaZr_{0.10}Ti_{0.90}O_3$, with the ∼715 and ∼780 cm^{-1} modes.

of the presence or absence of a ferroelectric phase [65, 66]. The relative intensity of these two modes (I_{715}/I_{780}) can thus be used as an indicator of the ferroelectric state of the material. Values of I_{715}/I_{780} much higher than unity would indicate a highly coherent long-range-ordered ferroelectric phase. Values closer to unity would indicate a system where the long-range ferroelectric order is largely disrupted. Values of 1 or lower would be indicative of a system where no long-range ferroelectric order is present at all. Figure 8 reports I_{715}/I_{780} plotted versus temperature for $BaZr_xTi_{1-x}O_3$ in the investigated temperature range. As can be seen in the figure, for BZT with $x = 0.10$ and $x = 0.20$ compositions the I_{715}/I_{780} intensity ratio initially decreases in a smooth manner with temperature, then takes an abrupt drop at 358 K and 298 K for $x = 0.10$ and $x = 0.20$, respectively, remaining constant with a value close to unity at higher temperatures. The temperatures at which the intensity drop occurs correspond to the maximum of the dielectric permittivity of the respective BZT ceramics, and are close to the ferroelectric-to-paraelectric transition temperatures reported in [15, 29, 32]. The overall (I_{715}/I_{780}) intensity ratio observed for BZT with $x = 0.20$ is lower than for BZT with $x = 0.10$, suggesting a lower degree of ferroelectricity in the former as compared to the latter ceramic. With the $x = 0.40$ BZT sample, the (I_{715}/I_{780}) intensity ratio is seen to remain constant and below one across the whole temperature range we investigated (see figure 8). This suggests that BZT with $x = 0.4$ is not ferroelectric and so does not exhibit a structural phase transition with changing temperature, in line with the findings of the Rietveld refinements of the XRD data.

3.3. Atomic PDF studies

Our conventional XRD and Raman data clearly showed that the BZT ceramics studied here exhibit a long-range polar ordering when $x \leq 0.20$, and a relaxor behaviour for larger values of x. In BZT relaxors the Zr/Ti cation off-centre displacements are correlated or partially correlated on limited length scales only

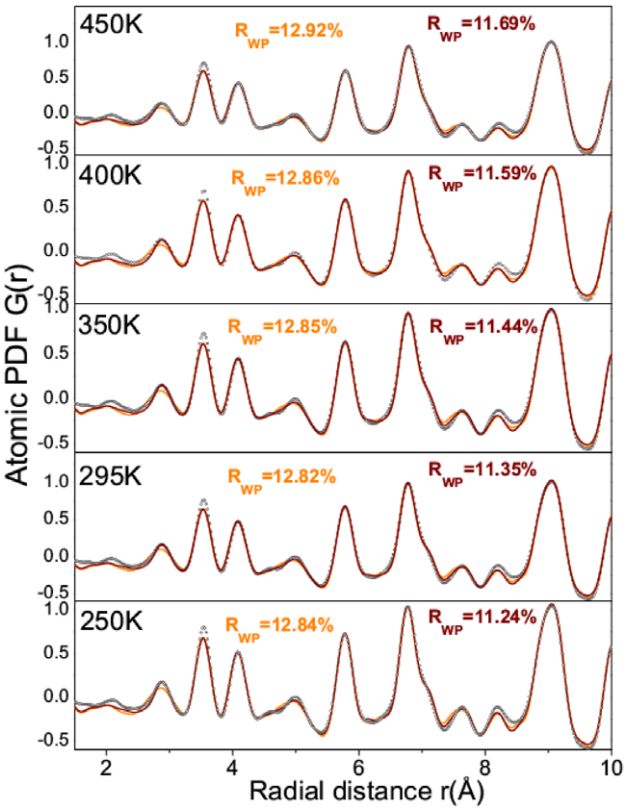

Figure 9. (a) Experimental (symbol), model 1 (brown line) and model 2 (orange line) PDFs for $BaZr_xTi_{1-x}O_3$ with $x = 0.10$. Data in the range of 1.5–10 Å are only shown for the sake of clarity. Model 1 data are computed strictly observing the constraints of a rhombohedral structure with $R3m$ symmetry. Model 2 data are computed on the basis of a cubic structure with $Pm3m$ symmetry.

within the PNRs, leading to zero macroscopic polarization. To access the presence of local Zr/Ti polar displacements and the PNRs associated with them, we fit the experimental PDFs with structure models featuring polar (rhombohedral/$R3m$) and non-polar (cubic/$Pm3m$) structure models. Results are shown in figures 9–11. Due to the property of Fourier transformation, experimental errors pile up close to the origin, i.e. at small values of the real space vector r. Since structure models testing and refinement does not take into account experimental errors, PDF fits to weak structural features appearing at low r values (e.g. at r values of approx. 2 Å) are rarely of a good quality. Fits to the experimental PDF data shown in figure 11 strictly obey the symmetry constraints of the tested rhombohedral- and cubic-type models, i.e. do not take into account the eventual presence of more subtle local structural distortions, and may explain the inferior quality of the constrained PDF fits at r values close to 6 Å.

The PDF fits for BZT with $x = 0.10$ and 0.20 based on the $R3m$ structure model turned out to be better than those based on the $Pm3m$ model for all temperatures covered by our studies, as documented by the better fit agreement factors R_{wp} ($x = 0.10$, average values: 11.46% for $R3m$, 12.86% for $Pm3m$; $x = 0.20$, average values: 13.24% for $R3m$, 15.97% for $Pm3m$). The result indicates the presence of local polar ordering in BZT with $x = 0.10$ and 0.20 even

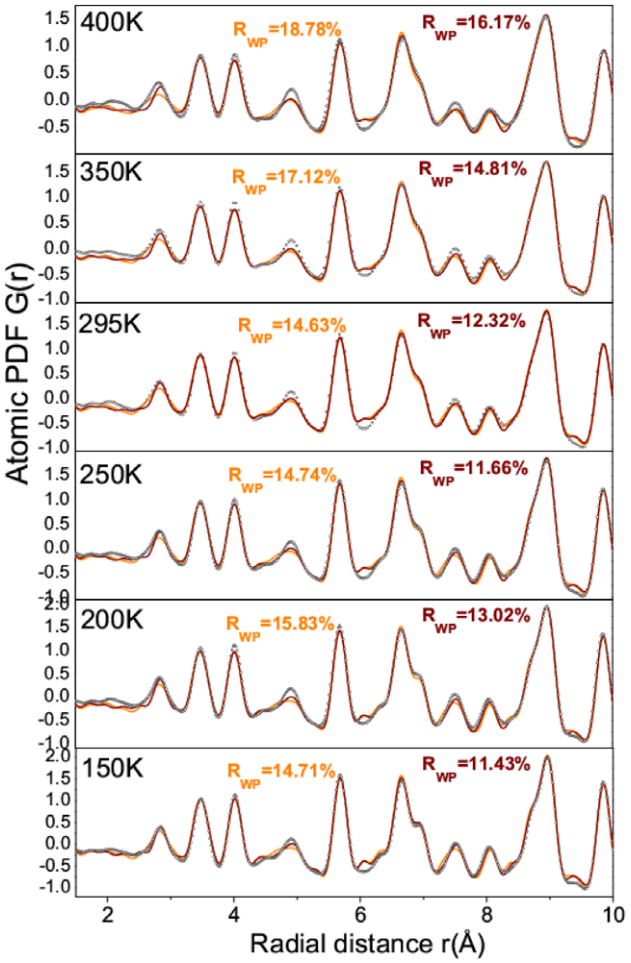

Figure 10. (a) Experimental (symbol), model 1 (brown line) and model 2 (orange line) PDFs for $BaZr_xTi_{1-x}O_3$ with $x = 0.20$. Data in the range of 1.5–10 Å are only shown for the sake of clarity. Model 1 data are computed strictly observing the constraints of a rhombohedral structure with $R3m$ symmetry. Model 2 data are computed on the basis of a cubic structure with $Pm3m$ symmetry.

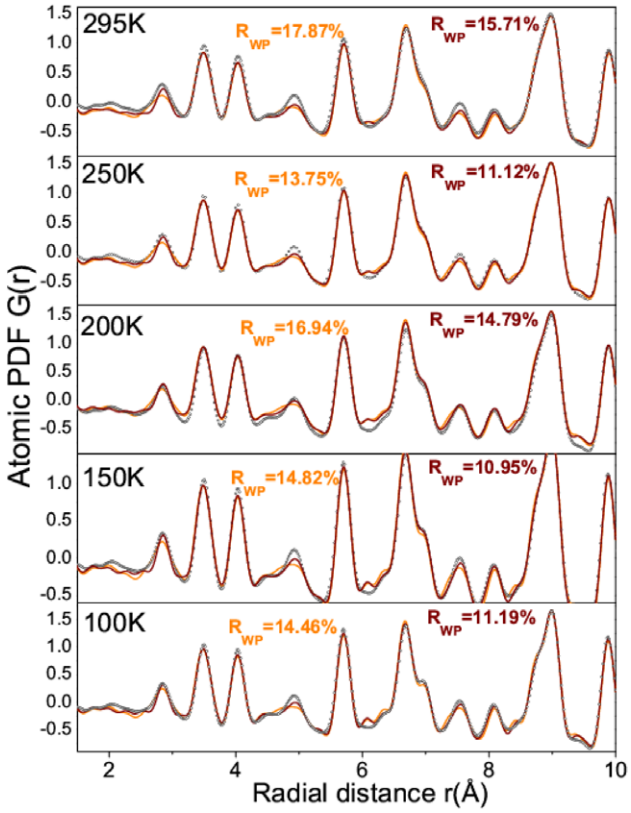

Figure 11. (a) Experimental (symbol), model 1 (brown line) and model 2 (orange line) PDFs for $BaZr_xTi_{1-x}O_3$ with $x = 0.40$. Data in the range of 1.5–10 Å are only shown for the sake of clarity. Model 1 data are computed strictly observing the constraints of a rhombohedral structure with $R3m$ symmetry. Model 2 data are computed on the basis of a cubic structure with $Pm3m$ symmetry.

at temperatures ($T \geq 360$ K for $x = 0.10$ and $T > 300$ K for $x = 0.20$) at which the average structure revealed by Rietveld analysis is cubic. Hence, our findings show that local polar clusters exist even in the paraelectric phase of average cubic symmetry, as also indicated by Raman scattering, despite the well-defined paraelectric-to-ferroelectric transition. For BZT with $x = 0.40$, again the PDF fits based on a polar $R3m$-type model (average R_{wp} 12.75%) are better than those based on a non-polar, cubic-type model (average R_{wp} 15.57%), indicating the coexistence of local polar ordering with the average cubic structure suggested by Rietveld analysis at all temperatures covered by our studies. For all BZT ceramics studied here, the differences in R_{wp} between the polar and non-polar models decrease with increasing temperature, suggesting that the local polar clusters are decreasing in size with increasing temperature.

In relaxor systems such as BZT with $x = 0.40$, the increase or decrease in size of PNRs can also be determined by Raman spectroscopy by monitoring the integrated intensity of the phonon mode at ~515 cm^{-1}. This is possible because the intensity is a function of the spatio-temporal auto-correlation function of the electronic polarizability [29]. When the PNRs grow, the integrated intensity of Raman modes is expected to increase, until a plateau is reached at the freezing temperature T_f, below which the nonergodic relaxor state is reached and the PNRs grow no further. Figure 12 shows the integrated intensity of the ~515 cm^{-1} mode for BZT with $x = 0.4$. It can be seen clearly that the intensity increases with decreasing temperature. This indicates that the size of polar clusters increases with decreasing temperature, in line with the findings of PDF analysis. The growth of PNRs is faster in the range 320–380 K and around 210 K. The freezing temperature for BZT with $x = 0.4$ resulting from figure 12 is close to 150 K, in agreement with other studies [29]. Assuming that the integrated intensity of the ~515 cm^{-1} Raman feature is proportional to the volume of the PNRs (supposed of spherical shape) it may be estimated that the PNR size in the frozen relaxor state is about two times larger than that in the non-frozen state at 450 K.

Both PDF analysis and Raman spectroscopy clearly indicate the existence of local PNRs at temperatures well above the ferroelectric-to-paraelectric transition in BZT ceramics with $x = 0.10$ and 0.20, and the evolution of PNR volume with decreasing temperature. In BZT with $x = 0.10$ and 0.20 this local polar order evolves in a long-range ferroelectric order on cooling through the Curie temperature. In BZT with

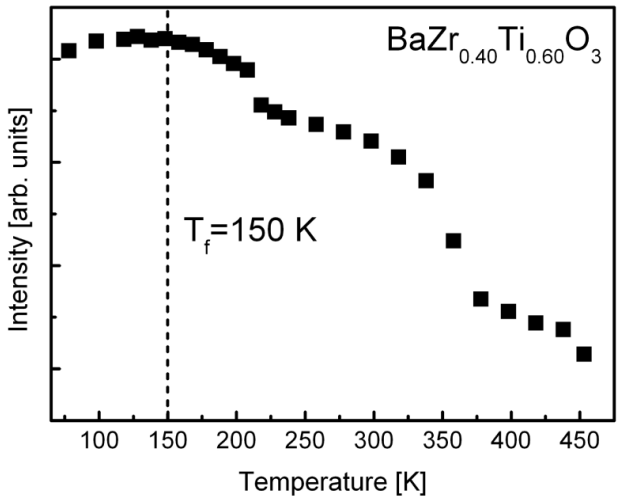

Figure 12. Integrated intensity of the Raman mode at ∼515 cm^{-1} for $BaZr_{0.40}Ti_{0.60}O_3$. The increasing intensity upon cooling is an indication of coarsening of the PNRs. A plateau is reached at 150 K. That temperature can be regarded as the freezing temperature (T_f) of PNRs in this ceramic.

$x = 0.4$ the long-range ferroelectric order does not appear on cooling, since PNRs are observed even at 100 K and the ceramics has, on average, cubic-type structure. It is to be noted that the PNRs are due to the off-centre displacement of Ti ions and the existence of local strain of the perovskite structure arising from the difference in the sizes of Zr and Ti cations. According to PDF analysis these local PNRs may be described in terms of a rhombohedral structural model. In lead-containing relaxors ($PbMg_{1/3}Nb_{2/3}O_3$) and in relaxors obtained by doping $BaTiO_3$ with heterovalent cations, PNRs are mostly due to compositional fluctuations which give rise to charge ordering and randomly oriented electric fields. However, the formation of PNRs in isovalent substituted $BaTiO_3$, such as $BaZr_xTi_{1-x}O_3$, has to be explained by a different mechanism. Isovalent substitution cannot lead to a local charge ordering and random electric fields. Our Raman data clearly show that the TiO_6 and ZrO_6 octahedra retain their individuality in the BZT ceramics, likely because of the rather large size difference between Ti^{4+} (0.605 Å) and Zr^{4+} (0.72 Å) cations, in good agreement with recent EXAFS and neutron scattering studies [58, 59]. According to first-principles calculations [75], the initial nucleation of PNRs in BZT at high temperature is driven by compositional fluctuations leading to spatial regions enriched in Ti inside which the elemental electric dipoles have the same direction. Further growth of these Ti-rich precursor PNRs is likely to be of thermodynamic origin and driven by the reduction of the local strain achieved with the coarsening of the PNRs in comparison to a random distribution of TiO_6 and ZrO_6 octahedra. It is clear that segregation of zirconium ions outside the PNRs can occur, leading to the formation of Zr-rich clusters, which will inhibit the growth of the Ti-rich PNRs in larger ferroelectric domains when the amount of Zr reaches a threshold value. The existence of Zr-rich clusters is well supported by the observation of some Raman bands specific to Ti-site substituted $BaTiO_3$. As Zr ions have a weak tendency to displace off-centre inside the ZrO_6 octahedra of the perovskite structure, the Zr-rich regions will be non-polar, or only weakly polar. In other words, the existence of Zr-rich clusters will disrupt the long-range ferroelectric order, especially in BZT with $x = 0.40$. Thus the relaxor state in $BaZr_xTi_{1-x}O_3$ with $x = 0.4$ will correspond to a random distribution of Ti-rich PNRs and Zr-rich non-polar clusters in a paraelectric matrix. With this mechanism, the crossover from a typical ferroelectric state to a relaxor state will require a high concentration of the homovalent substituent, between 20 and 40 at.% in the present case, and will be accompanied by a progressive reduction of the PNR correlation length.

4. Summary and conclusions

Average and local structure of $BaZr_xTi_{1-x}O_3$ ceramics (x = 0.1, 0.2 and 0.4) were investigated in the range of 100–450 K using several experimental techniques. The average BZT structure was determined by high-resolution synchrotron XRD and Rietveld refinements. Phase transitions in BZT and some aspects of the BZT local atomic-scale structure were revealed by Raman spectroscopy. In particular, when $x = 0.1$ all phase transitions typical of $BaTiO_3$ are observed in the temperature range 298–360 K. Only a diffuse rhombohedral–cubic transition occurs around room temperature for $x = 0.20$. The persistence of some polar bands in the Raman spectra of BZT with $x = 0.1$ and 0.2 collected well above the ferroelectric–paraelectric transition supports the existence of short-range correlated displacements on the B-sites of the perovskite structure, due to Ti-rich polar clusters inside a non-polar paraelectric matrix of average cubic-type structure. No phase transitions are observed for $x = 0.4$. The average cubic structure and the polar bands observed in BZT with $x = 0.4$ for all investigated temperatures correspond to a typical relaxor behaviour. In addition to the formation of polar clusters, Raman spectra also suggest a formation of Zr-rich clusters for all BZT compositions. Since $BaZrO_3$ is a paraelectric material, non-polar or weakly polar Zr-rich clusters may be expected in BZT ceramics. Analysis of the PDF data obtained from total x-ray scattering experiments indicates that a rhombohedral, polar-type structure model, corresponding to off-centre displacements of Ti ions along the [111] direction in the perovskite structure, describes quite well the local structure in BZT ceramics with x varying from 0.1 to 0.4. A non-polar, cubic-type structure model fails in this aspect. This gives extra evidence in support of the existence of polar nanoregions above T_C for BZT with $x = 0.1$ and 0.2, and in the whole investigated temperature range for BZT with $x = 0.4$. The polar clusters observed at high temperature for $x = 0.1$ and 0.2 evolve in a long-range ferroelectric order during cooling across the Curie temperature. In contrast, in BZT with $x = 0.4$, a long-range order does not develop, even at temperatures of the order of 100 K, although PNRs grow with decreasing temperature. Those, however, never reach a percolation threshold due to the existence of Zr-rich clusters. The growth of the PNRs in BZT with $x = 0.4$ is evidenced by the thermal behaviour of the intensity of the Raman band at 515 cm^{-1}. The intensity increases with decreasing temperature until a plateau is reached at ∼150 K, where a freezing of the PNRs takes place.

Acknowledgments

Use of the Advanced Photon Source at Argonne National Laboratory was supported by the US Department of Energy, Office of Science, Office of Basic Energy Sciences, under contract no. DE-AC02-06CH11357. The authors thank M Suchomel for the help with the high-resolution XRD experiments at beam-line 11-BM, Advanced Photon Source.

References

[1] Samara G A 2001 Ferroelectricity revisited—advances in materials and physics *Solid State Phys.* **56** 239
[2] Samara G A 2003 The relaxational properties of compositionally disordered ABO_3 perovskites *J. Phys.: Condens. Matter* **15** R367
[3] Shvartsman V V and Lupascu D C 2012 Lead-free relaxor ferroelectrics *J. Am. Ceram. Soc.* **95** 1
[4] Hennings D, Schnell A and Simon G J 1982 Diffuse ferroelectric phase transition in $Ba(Ti_{1-y}Zr_y)O_3$ ceramics *J. Am. Ceram. Soc.* **65** 539
[5] Hansen P, Hennings D and Schreinemacher H J 1998 Dielectric properties of acceptor-doped (Ba, Ca)(Ti, Zr)O_3 ceramics *J. Electroceram.* **2** 85
[6] Hansen P, Hennings D and Schreinemacher H J 1998 High-K dielectric ceramics from donor/acceptor-codoped $(Ba_{1-x}Ca_x)Ti_{1-y}Zr_y)O_3$ (BCTZ) *J. Am. Ceram. Soc.* **81** 1369
[7] Lee W H, Tseng T Y and Hennings D 2000 Effects of calcination temperature and A/B ratio on the dielectric properties of (Ba, Ca)(Ti, Zr, Mn)O_3 for multilayer ceramic capacitors with nickel electrodes *J. Am. Ceram. Soc.* **83** 1402
[8] Lee W H, Groen W A, Schreinemacher H and Hennings D 2000 Dysprosium doped dielectric materials for sintering in reducing atmospheres *J. Electroceram.* **5** 31
[9] Weber U, Greuel G, Boettger U, Weber S, Hennings D and Waser R 2001 Dielectric properties of Ba(Zr, Ti)O_3-based ferroelectrics for capacitor applications *J. Am. Ceram. Soc.* **84** 759
[10] Yu Z, Ang C, Guo R and Bhalla A S 2002 Dielectric properties and high tunability of $BaTi_{0.7}Zr_{0.3}O_3$ ceramics under dc electric field *Appl. Phys. Lett.* **81** 1285
[11] Dobal P S, Dixit A, Katiyar R S, Yu Z, Guo R and Bhalla A S 2001 Micro-Raman scattering and dielectric investigations of phase transition behavior in the $BaTiO_3$–$BaZrO_3$ system *J. Appl. Phys.* **89** 8085
[12] Miao S, Pokorny J, Pasha U M, Thakur O P, Sinclair D C and Reaney I M 2009 Polar order and diffuse scatter in $Ba(Ti_{1-x}Zr_x)O_3$ ceramics *J. Appl. Phys.* **106** 114111
[13] Kreisel J, Bouvier P, Maglione M, Dkhil B and Simon A 2004 High-pressure Raman investigation of the Pb-free relaxor $BaTi_{0.65}Zr_{0.35}O_3$ *Phys. Rev.* B **69** 092104
[14] Yu Z, Ang C, Guo R and Bhalla A S 2002 Ferroelectric-relaxor behavior of $Ba(Ti_{0.7}Zr_{0.3})O_3$ ceramics *J. Appl. Phys.* **92** 2655
[15] Maiti T, Guo R and Bhalla A S 2008 Structure–property phase diagram of $BaZr_xTi_{1-x}O_3$ system *J. Am. Ceram. Soc.* **91** 1769
[16] Sciau P, Calvarin G and Ravez J 1999 X-ray diffraction study of $BaTi_{0.65}Zr_{0.35}O_3$ and $Ba_{0.92}Ca_{0.08}Ti_{0.75}Zr_{0.25}O_3$ compositions: influence of electric field *J. Solid State Commun.* **113** 77
[17] Nagasawa M, Kawaji H, Tojo T and Atake T 2006 Absence of the heat capacity anomaly in the Pb-free relaxor $BaTi_{0.65}Zr_{0.35}O_3$ *Phys. Rev.* B **74** 132101
[18] Bokov A A, Maglione M and Ye Z G 2007 Quasi-ferroelectric state in $Ba(Ti_{1-x}Zr_x)O_3$ relaxor: dielectric spectroscopy evidence *J. Phys.: Condens. Matter.* **19** 092001
[19] Kleemann W, Miga S, Dec J and Zhai J 2013 Crossover from ferroelectric to relaxor and cluster glass in $BaTi_{1-x}Zr_xO_3$ ($x = 0.25$–0.35) studied by non-linear permittivity *Appl. Phys. Lett.* **102** 232907
[20] Egami T 2007 Local structure of ferroelectric materials *Annu. Rev. Mater. Res.* **37** 297
[21] Jeong I K, Arling T W, Lee J K, Proffen T, Heffner R H, Park J S, Hong K S, Dmowski W and Egami T 2005 Direct observation of the formation of polar nanoregions in $Pb(Mg_{1/3}Nb_{2/3})O_3$ using neutron pair distribution function analysis *Phys. Rev. Lett.* **94** 147602
[22] Güttler B, Mihailova B, Stosch R, Bismayer U and Gospodinov M 2003 Local phenomena in relaxor-ferroelectric $PbSc_{0.5}B''_{0.5}O_3$ ($B'' = Nb$, Ta) studied by Raman spectroscopy *J. Mol. Struct.* **661/662** 469
[23] El Marssi M, Le Marrec F, Lukyanchuk I A and Karkut M G 2003 Ferroelectric transition in an epitaxial barium titanate thin film: Raman spectroscopy and x-ray diffraction study *J. Appl. Phys.* **94** 3307
[24] Slodczyk A, Daniel P and Kania A 2008 Local phenomena of $(1-x)PbMg_{1/3}Nb_{2/3}O_3$–$xPbTiO_3$ single crystals ($0 <= x <= 0.38$) studied by Raman scattering *Phys. Rev.* B **77** 184114
[25] Kreisel J, Glazer A M, Bouvier P and Lucazeau G 2001 High-pressure Raman study of a relaxor ferroelectric: the $Na_{0.5}Bi_{0.5}TiO_3$ perovskite *Phys. Rev.* B **63** 174106
[26] Kreisel J, Bouvier P, Dkhil B, Thomas P A, Glazer A M, Welberry T R, Chaabane B and Mezouar M 2003 High-pressure x-ray scattering of oxides with a nanoscale local structure: application to $Na_{1/2}Bi_{1/2}TiO_3$ *Phys. Rev.* B **68** 014113
[27] Kim Y I, Page K, Limarga A M, Clarke D R and Seshadri R 2007 Evolution of local structures in polycrystalline $Zn_{1-x}Mg_xO$ ($0 <= x <= 0.15$) studied by Raman spectroscopy and synchrotron x-ray pair-distribution-function analysis *Phys. Rev.* B **76** 115204
[28] Aksel E, Forrester J S, Kowalski B, Deluca M, Damjanovic D and Jones J L 2012 Structure and properties of Fe-modified $Na_{0.5}Bi_{0.5}TiO_3$ at ambient and elevated temperature *Phys. Rev.* B **85** 024121
[29] Farhi R, El Marssi M, Simon A and Ravez J 1999 A Raman and dielectric study of ferroelectric $Ba(Ti_{1-x}Zr_x)O_3$ ceramics *Eur. Phys. J.* B **9** 599
[30] Dixit A, Majumder S B, Dobal P S, Katiyar R S and Bhalla A S 2004 Phase transition studies of sol–gel deposited barium zirconate titanate thin films *Thin Solid Films* **447** 284
[31] Karan N K, Katiyar R S, Maiti T, Guo R and Bhalla A S 2009 Raman spectral studies of Zr^{4+}-rich $BaZr_xTi_{1-x}O_3$ ($0.5 <= x <= 1.00$) phase diagram *J. Raman Spectrosc.* **40** 370
[32] Deluca M, Vasilescu C A, Ianculescu A C, Berger D C, Ciomaga C E, Curecheriu L P, Stoleriu L, Gajovic A, Mitoseriu L and Galassi C 2012 Investigation of the composition-dependent properties of $BaTi_{1-x}Zr_xO_3$ ceramics prepared by the modified Pechini method *J. Eur. Ceram. Soc.* **32** 3551
[33] Larson A C and Von Dreele R B 1994 General structure analysis system (GSAS) *Los Alamos National Laboratory Report LAUR 86-748*

[34] Toby B H 2001 EXPGUI, a graphical user interface for GSAS *J. Appl. Crystallogr.* **34** 210

[35] Petkov V 2008 Nanostructure by high-energy x-ray diffraction *Mater. Today* **11** 28

[36] Pradhan S K, Mao Y, Wong S S, Chupas P and Petkov V 2007 Atomic-scale structure of nanosized titania and titanate: particles, wires, and tubes *Chem. Mater.* **19** 6180

[37] Petkov V 1989 RAD, a program for analysis of x-ray diffraction data from amorphous materials for personal computers *J. Appl. Crystallogr.* **22** 387

[38] Tripathi S, Petkov V, Selbach S M, Bergum K, Einarsrud M A, Grande T and Ren Y 2012 Structural coherence and ferroelectric order in nanosized multiferroic $YMnO_3$ *Phys. Rev.* B **86** 094101

[39] Petkov V, Buscaglia V, Buscaglia M T, Zhao Z and Ren Y 2008 Structural coherence and ferroelectricity decay in submicron- and nano-sized perovskites *Phys. Rev.* B **78** 054107

[40] Jeong I-K, Mohiuddin-Jacobs F, Petkov V, Billinge S J L and Kycia S 2001 Local structure of $In_xGa_{1-x}As$ semiconductor alloys using high-energy synchrotron x-ray diffraction, *Phys. Rev.* B **63** 205202

[41] Comes R, Lambert M and Guinier A 1968 The chain structure of $BaTiO_3$ and $KNbO_3$ *Solid State Commun.* **6** 715

[42] Ravel B, Stern E A, Vedrinskii R I and Kraizmann V 1998 Local structure and the phase transitions of $BaTiO_3$ *Ferroelectrics* **206** 407

[43] Comes R, Lambert M and Guinier A 1970 Désordre linéaire dans les cristaux (cas du silicium, du quartz, et des pérovskites ferroélectriques) *Acta Crystallogr.* A **26** 244

[44] Zalar B, Laguta V V and Blinc R 2003 NMR evidence for the coexistence of order–disorder and displacive components in barium titanate *Phys. Rev. Lett.* **90** 037601

[45] Zalar B, Lebar A, Seliger J, Blinc R, Laguta V V and Itoh M 2005 NMR study of disorder in $BaTiO_3$ and $SrTiO_3$ *Phys. Rev.* B **71** 064107

[46] Simon A, Ravez J and Maglione M 2004 The crossover from a ferroelectric to a relaxor state in lead-free solid solutions *J. Phys.: Condens. Matter* **16** 963

[47] Burns G 1974 Lattice modes in ferroelectric perovskites. II. $Pb_{1-x}Ba_xTiO_3$ including $BaTiO_3$ *Phys. Rev.* B **10** 1951

[48] Tenne D A, Soukiassian A, Xi X X, Choosuwan H, Guo R and Bhalla A S 2004 Lattice dynamics in $Ba_xSr_{1-x}TiO_3$ thin films studied by Raman spectroscopy *J. Appl. Phys.* **96** 6597

[49] Buscaglia V *et al* 2005 Raman and AFM piezoresponse study of dense $BaTiO_3$ nanocrystalline ceramics *J. Eur. Ceram. Soc.* **25** 3059

[50] Teranishi T, Horiuchi N, Hoshina T, Takeda H and Tsurumi T 2010 Analysis on dipole polarization of $BaTiO_3$-based ferroelectric ceramics by Raman spectroscopy *J. Ceram. Soc. Japan* **118** 679

[51] Stern E A 2004 Character of order–disorder and displacive components in barium titanate *Phys. Rev. Lett.* **93** 037601

[52] Ostapchuk T, Pokorny J, Pashkin A, Petzelt J, Zelezny V, Rafaja D and Drbohlav I 2005 Soft-mode spectroscopy of $BaTiO_3$ thin films *J. Eur. Ceram. Soc.* **25** 3063

[53] Husson E 1998 Raman spectroscopy applied to the study of phase transitions *Key Eng. Mater.* **155/156** 3

[54] Zhong W, Vanderbilt D and Rabe K M 1994 Phase transitions in $BaTiO_3$ from first principles *Phys. Rev. Lett.* **73** 1861

[55] Loudon R 1964 The Raman effect in crystals *Adv. Phys.* **13** 423

[56] Merten L 1968 Zur Richtungsdispersion der optischen Gitterschwingungen des tetragonalen $BaTiO_3$ bei Zimmertemperatur *Phys. Status Solidi* **25** 125

[57] Jang M S, Takashige M, Kojima S and Nakamura T 1983 Oblique phonons with special concern to the soft phonon in tetragonal $BaTiO_3$ *J. Phys. Soc. Japan* **52** 1025

[58] Levin I, Cockayne E, Krayzman V, Woicik J C, Lee S and Randall C A 2011 Local structure of Ba(Ti, Zr)O_3 perovskite-like solid solutions and its relation to the band-gap behavior *Phys. Rev.* B **83** 094122

[59] Laulhe C, Hippert F, Bellissent R and Cuello G J 2009 Local structure in $BaTi_{1-x}Zr_xO_3$ relaxors from neutron pair distribution function analysis *Phys. Rev.* B **79** 064104

[60] Petzelt J and Dvorak V 1976 Changes of infrared and Raman spectra induced by structural phase transitions. I. General considerations *J. Phys. C: Solid State Phys.* **9** 1571

[61] Petzelt J and Dvorak V 1976 Changes of infrared and Raman spectra induced by structural phase transitions. II. Examples *J. Phys. C: Solid State Phys.* **9** 1587

[62] Kreisel J, Glazer A M, Jones G, Thomas P A, Abello L and Lucazeau G 2000 An x-ray diffraction and Raman spectroscopy investigation of A-site substituted perovskite compounds: the $(Na_{1-x}K_x)_{0.5}Bi_{0.5}TiO_3$ ($0 \leq x \leq 1$) solid solution *J. Phys.: Condens. Matter* **12** 3267

[63] Robins L H, Kaiser D L, Rotter L D, Schenck P K, Stauf G T and Rytz D 1994 Investigation of the structure of barium titanate thin-films by Raman spectroscopy *J. Appl. Phys.* **76** 7487

[64] Sakashita T, Deluca M, Yamamoto S, Chazono H and Pezzotti G 2007 Stress dependence of the Raman spectrum of polycrystalline barium titanate in presence of localized domain texture *J. Appl. Phys.* **101** 123517

[65] Feteira A, Sinclair D C and Kreisel J 2010 Average and local structure of $(1-x)BaTiO_3$–$xLaYO_3$ ($0 \leq x \leq 0.50$) ceramics *J. Am. Ceram. Soc.* **93** 4174

[66] Scalabrin A, Chaves A S, Shim D S and Porto S P S 1977 Temperature dependence of the A1 and E optical phonons in $BaTiO_3$ *Phys. Status Solidi* b **79** 731

[67] Fleury P A and Lazay P D 1971 Acoustic—soft-optic mode interactions in ferroelectric $BaTiO_3$ *Phys. Rev. Lett.* **26** 1331

[68] Venkateswaran U D, Naik V M and Naik R 1998 High-pressure Raman studies of polycrystalline $BaTiO_3$ *Phys. Rev.* B **58** 14256

[69] Gajović A, Vukailović Pleština J, Žagar K, Plodinec M, Šturm S and Čeh M 2013 Temperature-dependent Raman spectroscopy of $BaTiO_3$ nanorods synthesized by using a template-assisted solgel procedure *J. Raman Spectrosc.* **44** 412

[70] Lu D Y, Sun X Y and Toda M 2007 A novel high-k 'Y5V' barium titanate ceramics co-doped with lanthanum and cerium *J. Phys. Chem. Solids* **68** 650

[71] Deluca M, Stoleriu L, Curecheriu L P, Horchidan N, Ianculescu A C, Galassi C and Mitoseriu L 2012 High-field dielectric properties and Raman spectroscopic investigation of the ferroelectric-to-relaxor crossover in $BaSn_xTi_{1-x}O_3$ ceramics *J. Appl. Phys.* **111** 084102

[72] Strathdee T, Luisman L, Feteira A and Reichmann K 2011 Ferroelectric-to-relaxor crossover in $(1-x)BaTiO_3$–$xBiYbO_3$ ($0 \leq x \leq 0.08$) ceramics *J. Am. Ceram. Soc.* **94** 2292

[73] Schileo G, Luisman L, Feteira A, Deluca M and Reichmann K 2013 Structure–property relationships in $BaTiO_3$–$BiFeO_3$–$BiYbO_3$ ceramics *J. Eur. Ceram. Soc.* **33** 1457

[74] Bokov A A and Ye Z G 2006 Recent progress in relaxor ferroelectrics with perovskite structure *J. Mater. Sci.* **41** 31

[75] Akbarzadeh A R, Prosandeev S, Walter E J, Al-Barakaty A and Bellaiche L 2012 Finite-temperature properties of Ba(Zr, Ti)O_3 relaxors from first principles *Phys. Rev. Lett.* **108** 257601